sustainability

MDPI

Article

Modeling Permafrost Distribution Using Geoinformatics in the Alaknanda Valley, Uttarakhand, India

Arvind Chandra Pandey [1], Tirthankar Ghosh [1], Bikash Ranjan Parida [1,*], Chandra Shekhar Dwivedi [1] and Reet Kamal Tiwari [2]

[1] Department of Geoinformatics, School of Natural Resource Management, Central University of Jharkhand, Ranchi 835222, India
[2] Department of Civil Engineering, Indian Institute of Technology Ropar, Ropar 140001, India
* Correspondence: bikash.parida@cuj.ac.in

Abstract: The Indian Himalayan region is experiencing frequent hazards and disasters related to permafrost. However, research on permafrost in this region has received very little or no attention. Therefore, it is important to have knowledge about the spatial distribution and state of permafrost in the Indian Himalayas. Modern remote sensing techniques, with the help of a geographic information system (GIS), can assess permafrost at high altitudes, largely over inaccessible mountainous terrains in the Himalayas. To assess the spatial distribution of permafrost in the Alaknanda Valley of the Chamoli district of Uttarakhand state, 198 rock glaciers were mapped (183 active and 15 relict) using high-resolution satellite data available in the Google Earth database. A logistic regression model (LRM) was used to identify a relationship between the presence of permafrost at the rock glacier sites and the predictor variables, i.e., the mean annual air temperature (MAAT), the potential incoming solar radiation (PISR) during the snow-free months, and the aspect near the margins of rock glaciers. Two other LRMs were also developed using moderate-resolution imaging spectroradiometer (MODIS)-derived land surface temperature (LST) and snow cover products. The MAAT-based model produced the best results, with a classification accuracy of 92.4%, followed by the snow-cover-based model (91.9%), with the LST-based model being the least accurate (82.4%). All three models were developed to compare their accuracy in predicting permafrost distribution. The results from the MAAT-based model were validated with the global permafrost zonation index (PZI) map, which showed no significant differences. However, the predicted model exhibited an underestimation of the area underlain by permafrost in the region compared to the PZI. Identifying the spatial distribution of permafrost will help us to better understand the impact of climate change on permafrost and its related hazards and provide necessary information to decision makers to mitigate permafrost-related disasters in the high mountain regions.

Keywords: permafrost; logistic regression model; rock glacier; Indian Himalayas

check for updates

Citation: Pandey, A.C.; Ghosh, T.; Parida, B.R.; Dwivedi, C.S.; Tiwari, R.K. Modeling Permafrost Distribution Using Geoinformatics in the Alaknanda Valley, Uttarakhand, India. *Sustainability* **2022**, *14*, 15731. https://doi.org/10.3390/su142315731

Academic Editor: Chunlin Song

Received: 22 September 2022
Accepted: 23 November 2022
Published: 25 November 2022

1. Introduction

Permafrost is the subground material (soil and rock) that remains below 0 °C for at least two consecutive years [1]. It is an integral part of the cryosphere and is considered an important indicator of climate change. The thickness of the permafrost varies from 1 m to 1500 m in some places [2]. The World Meteorological Organization (WMO), under the Global Climate Observing System (GCOS), designates permafrost as one of the essential climatic variables (ECVs) under the category of the cryosphere, along with glaciers, snow, ice sheets, and ice shelves [3]. It affects the soil moisture and the landscape over a large area, has a strong relationship with the hydrological, biological, and geomorphic processes, and affects the anthroposphere [4,5]. As the global average air temperature rises, permafrost in mountain regions is expected to undergo degradation and thaw in the coming decades [6]. The thawing of permafrost can have multiple effects, and some of the critical impacts are ground subsidence and an increased frequency of landslides due to the destabilization of grounds and slopes [7]. The latter will negatively influence infrastructure such as bridges, roads, and buildings, along with an increase in sediment load during runoff into rivers [8,9]. One such event which took place in the Chamoli district of Uttarakhand in February 2021, where a considerable mass of a rock–ice complex collapsed from an unstable mountain slope, resulting in a catastrophic mass flow of debris, which was linked to the possible degradation of permafrost [10]. As the climate is warming up, such hazardous events are likely to happen often. In the last few decades, the region has experienced multiple bouts of natural hazards and disasters, such as ice–rock avalanches, landslides, slope failures, and rock falls, which may be linked to the possible degradation of permafrost [10,11]. Several major landslides have occurred in the Indian Himalayan region that damaged infrastructure and resources over the years [11], the most well-known ones being the Lanta Khola landslide (1975); Malpa landslide (1998); Phata landslide (2001); Varunavat landslide (2003); Pithoragarh landslide (2009); Okhimath landslide (2012); Tangni landslide (2013); Kotropi landslide (2017); and Chamoli disaster (2021). A massive moraine-dammed lake (i.e., Chorabari Glacier) breached in 2013 in Kedarnath, Uttarakhand, following heavy rainfall and snowmelt and triggered a debris flow upstream that devastated major infrastructure along the Mandakini river [12]. A recent massive avalanche in October 2022 in Uttarkashi, Uttarakhand, killed at least 27 mountaineers of the Nehru Institute of Mountaineering (NIM) and injured several others as they were trapped under snow or fell into crevasses in the glacier. The chain of such events emphasizes the rising risk in the Himalayas as a result of global warming and industrialization [10,13]. Therefore, it is necessary to have an extensive understanding of the spatial arrangement of permafrost and its current state of existence.

The prediction and estimation of the permafrost distribution in high mountainous regions have frequently been linked with rock glaciers, which are considered to be the most prominent indicators of permafrost in an alpine setting [14,15]. Rock glaciers are cryospheric lobate-shaped features formed by the gravity-driven creep of ice-oversaturated talus or tills. Their characteristic features include ridge and furrow topography that has been caused due to longitudinal compression and folding because of their creeping nature [16,17]. Based on the activeness and permafrost content of rock glaciers, they have been majorly categorized into active (containing ice and moving) and relict rock glaciers (not containing ice and not moving). All these features can easily be identified and mapped on high-resolution satellite images. Therefore, it is crucial to understand the occurrence and spatial locations of rock glaciers and their activity. While there have been numerous studies on glaciers and glacier-related hazards and processes in the Indian Himalayas, such as [18–22], the science of permafrost is still very much under-researched in the region.

The statistical modeling of rock glaciers and their relationship with climatic conditions near rock glacier sites has been used to predict the permafrost distribution in various regions of the world [23–25]. Most of the studies related to permafrost and its dynamics are focused on the polar region and some European highlands, but there are very few studies and explorations related to permafrost as far as the Indian Himalayan region is concerned. There have been quite a number of studies conducted in the region of the Qinghai–Tibet Plateau [5,26]. A few studies have focused on the Hindu Kush Himalayan (HKH) region and demonstrated permafrost distribution modeling, issues related to the permafrost thaw in the mountains, and the assessment of published permafrost distribution maps based on rock glaciers [27–29]. An inventory of rock glaciers and an estimation of the permafrost distribution in the state of Uttarakhand, India, based on rock glaciers and climatic variables was initially attempted by Baral et al. [30]. Another study of permafrost mapping mainly focused on the Kullu District of Himachal Pradesh in the Western Himalayas and concluded that around 9% of the total area of the Kullu district is underlain by permafrost, where the lower limit of permafrost is as low as ~4200 m [31]. Haq and Baral [32] performed an assessment and inventory of rock glacier and permafrost mapping in the Sikkim Himalayas using Sentinel-2 data and logistic regression modeling. A recent study by Khan et al. [33] used remote sensing techniques coupled with ground validations to quantify the permafrost distribution in parts of the Western Himalayas. Most of the above studies conducted in the Indian Himalayan region were based on the analytical hierarchical process (AHP) and statistical modeling using parameters, namely air temperature, potential incoming solar radiation (PISR), slope, aspect, and land use/land cover [30–33]. However, the aforementioned studies have ignored the influence of snow cover on permafrost distribution and lack comparisons among models considering different climate parameters such as the mean annual air temperature (MAAT), land surface temperature (LST), and snow cover (SC). Moreover, previous studies were conducted using remote sensing satellite data with lower spatial resolutions [34,35], implying that a higher spatial resolution dataset is required for an improvement in predicting rock glaciers and permafrost models. The Indian Himalayan region also needs more studies on permafrost to understand its behavior under perceived climate changes in the higher Himalayan regions [36].

The present study is aimed to identify several rock glaciers in the Alaknanda Valley region in the Uttarakhand state of India. Using mapped rock glaciers, different models were developed based on logistic regressions to predict the spatial arrangement of permafrost in the study area with a higher spatial resolution (30 m). All the models were further evaluated and compared to understand their efficiency and reliability. The rest of the paper is organized as follows: Section 2 describes the study area. Section 3 describes the data and models used in the present study. The results and discussion are presented in Sections 4 and 5, respectively. Finally, the conclusion of the study is given in Section 6.

2. Study Area

This study focuses on the part of the Alaknanda Valley in the Uttarakhand state of India, covering an area of 11,318 km^2. The Alaknanda River originates at the confluence of the Satopanth and Bhagirathi Kharak glaciers at an elevation of ~3800 m, 13 km north of the Badrinath temple in the Chamoli district. Some well-known spots such as Kedarnath, Badrinath, Mana, Joshimath, etc., are also in this region. The Saraswati, Dhauliganga, Goriganga, Patalganga, Birehiganga, Nandakini, and Pindar streams join the Alaknanda River on the left bank, and it is joined on the right bank by the Mandakini. The area is surrounded by high mountain peaks such as Mt. Chaukhamba (7138 m), Mt. Nilkantha (6596 m), Mt. Satopanth (7075 m), and Nar Parvat (5801 m). The Alaknanda and the Saraswati River converge near the village of Mana. The upper basin of the Alaknanda Valley consists of glaciers, glacial lakes, moraines, avalanche slopes, etc., which are some of the common landforms of the region. The cumulative liquid precipitation in the region varies from 500 to 1500 mm per annum, whereas the yearly snowfall in the study area ranges from 1 to 8 mm of water equivalent per annum (summer to winter). A map of the study area is shown in Figure 1.

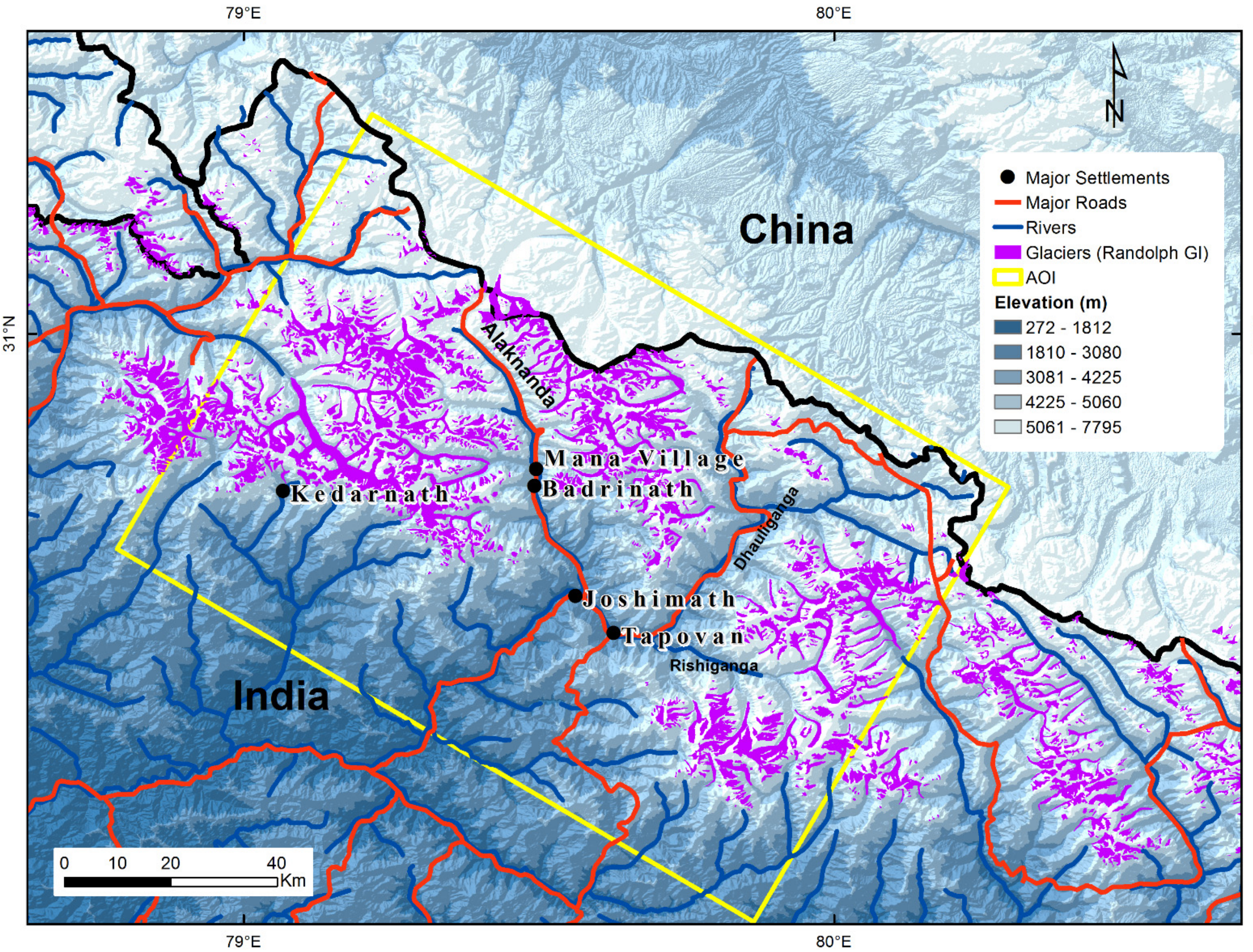

Figure 1. Study area map showing major settlements, rivers, glaciers, and road networks in the Alaknanda Valley region, along with elevations.

3. Materials and Methods

3.1. Data Used

To develop a permafrost zonation map for the study area, the rock glaciers in the region were identified and mapped. Rock glaciers, based on their activity, constitute an indicator of the presence or absence of permafrost. After that, a statistical relationship was developed between the permafrost and topoclimatic variables (predictor variables) such as the mean annual air temperature (MAAT), the potential incoming solar radiation (PISR), and the aspect of the slope where rock glaciers are present, which provided a predicted spatial distribution of permafrost in the study area. Two other models were also developed using land surface temperature (LST) and snow cover data for the area. The details of the data are described in Table 1.

Table 1. Details of the data used in this study.

Dataset Used	Spatial/Temporal Resolution	Purpose	Source
WorldClim Average Temperature	~1 km/monthly	to develop MAAT layer	[37]
MODIS LST	1 km/8 days	to develop mean LST layer	[38]
MODIS Snow Cover	500 m/daily	to develop mean snow cover layer	[39]
ASTER GDEM	30 m/NA	to develop PISR and aspect layers	[40]
GTOPO 30	~1 km/NA	to develop MAAT layer	[41]

3.2. Predictor Variables

3.2.1. Mean Annual Air Temperature (MAAT)

MAAT data were obtained from WorldClim version 2, a freely available global climate database. The bioclimatic variables in the WorldClim version 2 data are the averages of all the monthly data for the period of 1970–2000, which can be used for mapping and spatial modeling [37]. They have a spatial resolution of ~1 km^2 and a temporal resolution of 1 month.

To develop a ~30 m resolution MAAT grid from the ~1 km resolution MAAT layer, a technique described by Marcer et al. [24] was followed. A linear regression between MAAT and GTOPO30 (~1 km resolution) [41] was performed to generate a lapse rate layer (1 km). Lapse rates were computed locally for each grid cell at a 1 km resolution by evaluating the linear relationship between the surrounding temperatures and the elevation data. These layers were then resampled with the bilinear interpolation method (i.e., each pixel in the resampled raster was the result of the four neighboring input pixels) to match the grid size of the Advanced Spaceborne Thermal Emission and Reflection Radiometer (ASTER) Global Digital Elevation Model (GDEM) Version 3 (30 m spatial resolution) [40]. In the bilinear interpolation, all layers were converted from their native resolution (Table 1) to a 30 m spatial resolution. Two DEM layers, the resampled GTOPO30 (resampled at ~30 m) and ASTER GDEM v3 (~30 m), were compared. The elevation difference layer and the resampled lapse rate layer were multiplied, and the resulting raster layer was then added to the resampled MAAT grid to generate the ~30 m MAAT grid for further processing.

3.2.2. Land Surface Temperature (LST)

For another logistic regression model, the LST layer was developed from the MODIS-based Land Surface Temperature and Emissivity 8-Day Global 1km (MOD11A2.061) dataset [38]. These data give an average of 8 days per pixel of LST and emissivity with a spatial resolution of 1 km. It comprises both the daytime and nighttime surface temperature data. Various studies in the past have used MODIS-based LST to predict permafrost in their study areas [42–44]. As permafrost is a subsurface material, LST has an effect on the state of the permafrost and its spatial arrangement within the region. As no in situ data on ground temperature were available for the study, LST was considered as one of the independent variables for the model.

To generate the LST raster layer, the means of 21 years (2000–2020) of data were considered for the LST daytime and LST nighttime data bands, and further means of both these layers were estimated. Finally, they were exported to the system from the cloud with a scale of 1000 m and projected to World Geodetic System 84 (WGS 84) for further analysis. All this processing was performed on the Google Earth Engine (GEE) platform for the specified study area boundary to reduce the processing time and efficiently generate the output from the bulk data. Thereafter, a similar methodology was used to generate a ~30 m spatial resolution for the LST grid, as in the case of the MAAT. In this case, the MAAT layer was replaced with the MODIS LST layer (~1 km resolution).

3.2.3. Snow Cover

Snow cover data for the study area were also considered for developing an additional logistic regression model, as a study suggested that mountain permafrost distribution is strongly controlled by local climatic conditions, especially snow cover [45]. We used MODIS Terra Snow Cover Daily Global 500m (MOD10A1.006) data to develop the snow cover layer [39]. They contained a gridded dataset of snow cover and snow albedo calculated from the radiance data acquired by the MODIS Terra satellite. The normalized difference snow index (NDSI) was computed to detect snow cover from the MODIS Level 1B calibrated radiance satellite images [46]. Their spatial resolution was 500 m, and they were available from the 24th of February 2000 to the time of data collection.

Similar to LST, means of 21 years (2000–2020) of snow cover data were used to develop the snow cover layer. The snow cover data were imported from the GEE repository to process on the cloud platform. The MODIS Terra Snow Cover data has various datasets in separate bands such as "NDSI_Snow_Cover", "NDSI_Snow_Cover_Basic_QA", "NDSI", etc., which have different uses. Here, we used the "NDSI_Snow_Cover" band to retrieve a fractional snow cover layer whose values ranged from 0 to 100. After calculating the mean, the raster data were exported to the system from the cloud with a spatial resolution of 1000 m and were projected to WGS84. In the end, a similar technique was used to develop the ~30 m spatial resolution gridded layer, this time replacing the MAAT layer with the snow cover data layer.

3.2.4. Potential Incoming Solar Radiation (PISR)

The incoming solar radiation was calculated based on the 30 m ASTER GDEM v3 [40] on ArcMap using the 'Area Solar Radiation' tool. A snow-free period from the 1st of May to the 31st of October was considered to estimate the PISR, as the incoming radiation has an effect on the ground temperatures during the low-albedo season [47], and this period is considerably snow-free in the region of Uttarakhand [48,49]. All the values were kept as their defaults, except the sky size value, which was set to 512. Under the radiation parameter "Uniform Sky", the diffused model was selected. The output values were in Watt hours per square meter (Wh m^{-2}), which was later converted to kilowatt hours per square meter (KWh m^{-2}) for further analysis and logistic regression modeling

3.2.5. Aspect

The aspect of the rock glacier slopes was also considered in the model, as it decides the insolation intensity and the response of the snowpack towards it and climate warming [50]. The aspect layer was generated from the ASTER DEM (30 m resolution) using the "Aspect (Spatial Analyst tool)" in ArcMap.

After processing all the data required for the logistic regression modeling, a database of active and relict rock glaciers was developed with the corresponding values of topoclimatic variables (MAAT, LST, snow cover, PISR, and aspect) at the initiation line of the respective rock glaciers. For each initiation point, values from different topographic attribute layers were extracted using the 'Extract Multi Values to Points' tool in ArcMap.

Raster layers of all the predictor variables used in this study to model permafrost are shown in Figure 2.

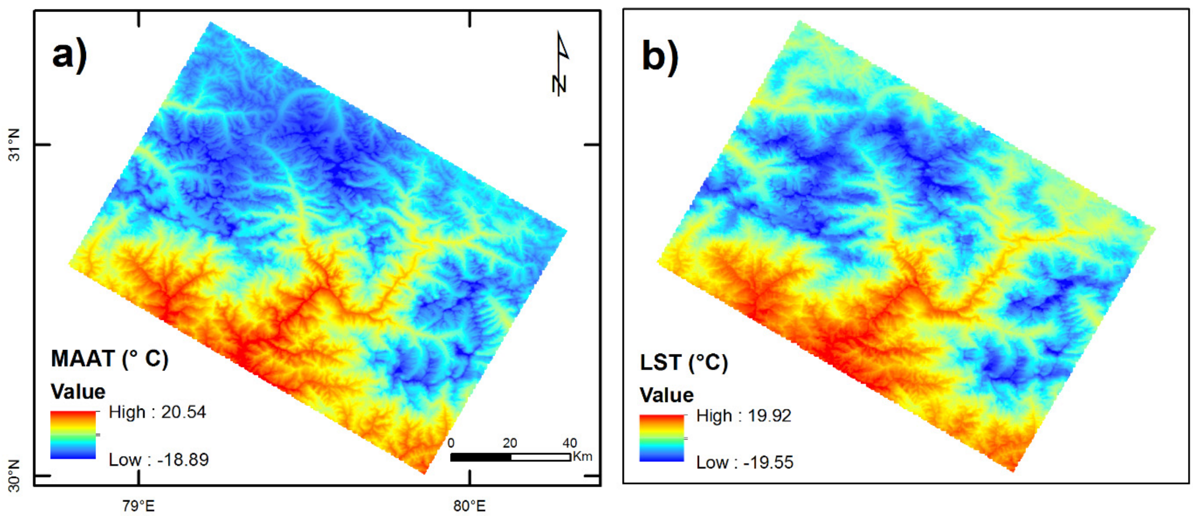

Figure 2. *Cont.*

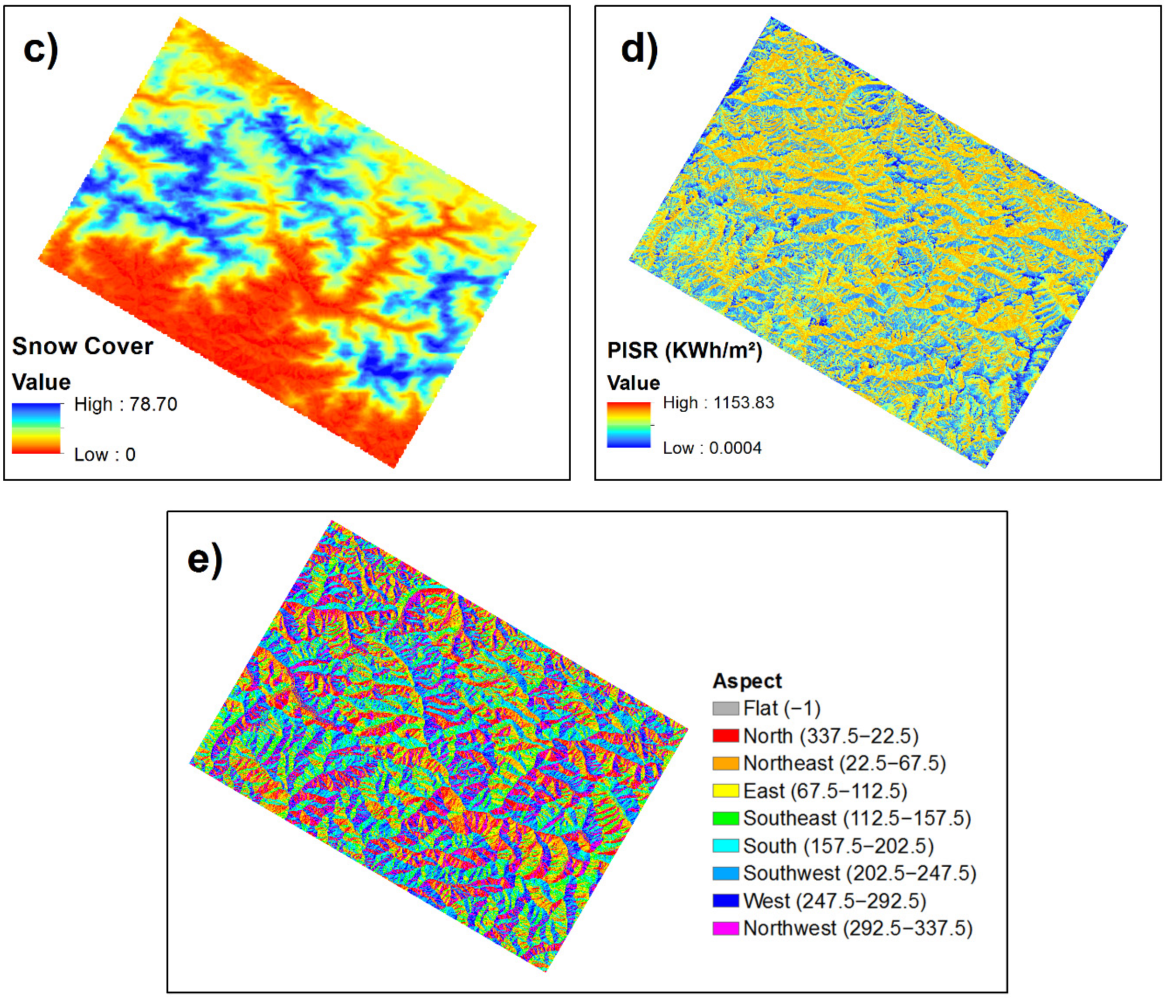

Figure 2. Different predictor variables used in the logistic regression models. Specifically, (**a**) displays the mean MAAT for 1970–2000; (**b**,**c**) display the means of LST and snow cover for 2000–2020, respectively; (**d**) displays the PISR for snow free period; (**e**) displays the slope aspect of the study area.

3.3. Methodology

3.3.1. Identification and Mapping of Rock Glaciers

The rock glaciers were manually identified and digitized from high-resolution satellite data such as SPOT and Digital Globe (e.g., QuickBird, Worldview-1, Worldview 2, and IKONOS), which are freely available on the Google Earth platform. The availability of past multitemporal satellite images also helped with better identifying rock glaciers and lowered the uncertainty due to cloud cover, shadow, and snow in a different dataset. The study area shapefile was exported as a Keyhole Markup Language (KML) file and imported to Google Earth Pro. It was then divided into 12 grids for better investigation and a thorough inspection of the whole study area. The rock glacier boundaries were digitized, along with their initiation points or 'rooting zone' [14], i.e., from where permafrost creep actually begins. All the mapped features were exported as KML files and were further processed for spatial analysis in GIS.

In this study, on the basis of their activeness, rock glaciers were categorized as active (Figure 3) or relict (Figure 4) and were identified and digitized following the visual interpretation keys and morphological characteristic features of each rock glacier. The rock glaciers with ridge and furrow topography were characterized as active rock glaciers, while those with less prominent ridge–furrow topography were classified as relict rock glaciers. Some rock glaciers with a prominence of ice on the surface in some places were classified as active, whereas the relict rock glaciers lacked such features. All the rock glaciers were given a unique ID, and in the description their type was mentioned to avoid any error in further analyses. Landform features similar to the morphology of rock glaciers, such as moraines or landslide debris, were distinguished carefully. Therefore, those landform features that expressed the characteristic features of permafrost origin were mapped. The three-dimensional (3D) terrain viewing tool on Google Earth Pro was very useful in understanding the origin and occurrence of rock glaciers. A summary of the visual interpretation keys that were used is given in Table 2.

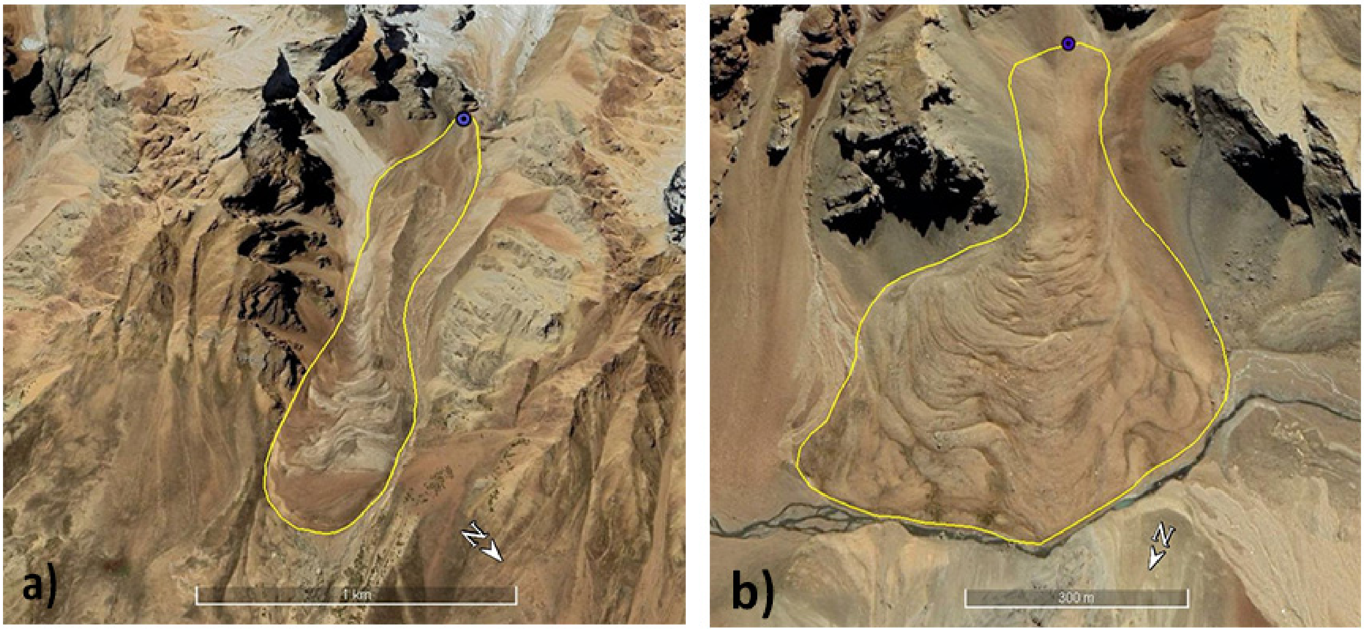

Figure 3. (**a**,**b**) Active rock glaciers mapped on Google Earth Pro (blue circles signify their initiation points).

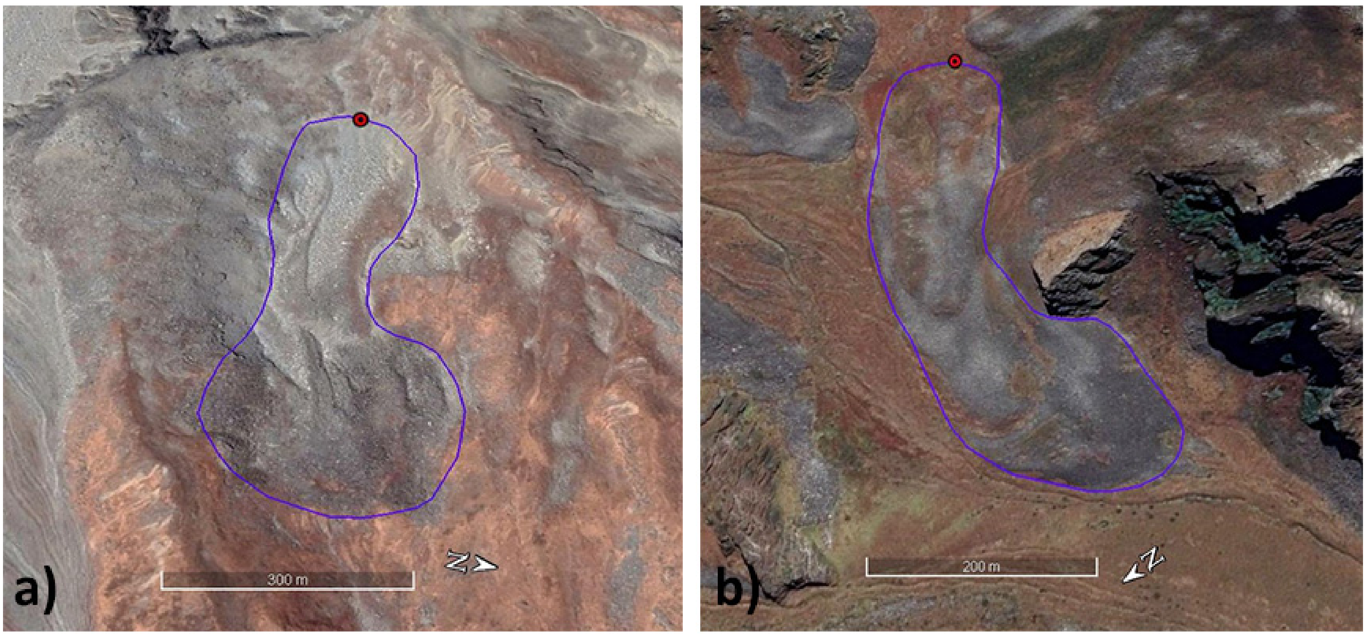

Figure 4. (**a**,**b**) Relict rock glaciers mapped on Google Earth Pro (red circles signify their initiation points).

Table 2. Characteristic features of rock glaciers utilized for visual identification in satellite images.

Geomorphic Indicators	Active	Relict
Surface structure	Prominent furrow and ridge topography [51]	Less prominent furrow and ridge topography [51]
Body	Bulged swollen structure [52] Exposure of ice on the surface in some places [53]	Flat and subdued surface topography [52] Deflated surface feature [54]
Frontal Lobe	Sharp-crested frontal lobe slope [55]	Gentle transition from frontal lobe to body [55]

In the present study, the initiation points of the active rock glaciers were considered as an indication of the presence of permafrost [25,56], as the climatic conditions that support the presence of ice-rich permafrost are primarily found in these zones. In alignment with previous studies [23,25,57], relict rock glaciers were considered as evidence of permafrost absence. While digitizing their initiation point, in some cases it was observed that there are no clear markings or visible rooting zones because of the presence of vegetation and subdued surface topography. Therefore, an approach similar to that mentioned by Marcer et al. [24] was taken into consideration, where the centroid of the polygon for relict rock glaciers was chosen for the statistical modeling (Figure 4).

3.3.2. Logistic Regression Model

A logistic regression model is a statistical method that predicts a binary outcome or predicts the conditional probability of a dichotomous outcome (variable *Y*) occurring (e.g., the presence of permafrost (1) or the absence of permafrost (0)) based on a set of independent variables (*X*) [58], which are also called predictors [59]. A logistic regression fits an "S" shaped logistic function that predicts the variable's two maximum values, 0 or 1. It gives a probabilistic value that ranges between 0 and 1 (the absence of permafrost and the presence of permafrost).

Mathematically, a logistic regression can be expressed as

$$P(Y=1) = \frac{e^{\beta_0+\beta_1 x_1+\beta_2 x_2+\ldots\beta_n x_n}}{1+e^{\beta_0+\beta_1 x_1+\beta_2 x_2+\ldots\beta_n x_n}} \quad (1)$$

where $P(Y = 1)$ is the probability of outcome Y taking the value 1; β_0 is the intercept; β_n is the coefficient of the predictor variables X_n; and e is the base of the natural logarithm, which has a value of 2.71828.

Logistic regression modeling (LRM) has been used in numerous previous studies to estimate the permafrost distributions in different high mountain regions of the world [23–25,30,32]. In this study, a total of three models were developed based on different climate parameters, the mean annual air temperature (LRM-MAAT), the land surface temperature (LRM-LST), and snow cover (LRM-SC), along with the PISR and the aspect as the common parameters in all the three models.

All three LRMs were developed in the IBM SPSS Statistics tool. Furthermore, all the operations on the GIS layers were performed using the raster calculator in ArcMap to generate the permafrost distribution map using the coefficient outputs from the models and substituting them in Equation (1). To measure the performance of all the LRMs, the area under receiver operating characteristics (ROC) curve was calculated using the IBM SPSS tool. The bias and standard error (SE) were also calculated to indicate the robustness and performance of the different models.

4. Results

4.1. Rock Glacier Compilation

The present study identified a total of 199 rock glaciers, out of which 183 (91.95%) were active rock glaciers and 15 (8.05%) were mapped as relict rock glaciers. The lowest elevation at which an active rock glacier was found was 4270 m, whereas a relict glacier was found at 4027 m. Most of the active rock glaciers in the study area were glacier-derived rock glaciers, and a few were talus-derived, which signifies the retreat of small glaciers due to continuous negative mass balance in the region.

The temperature and orientation of the rock glaciers have a significant effect on the present state and activity of the rock glaciers. The maximum number (N = 80) of active rock glaciers was found in the elevation band of 4800–5200 m, as shown in Figure 5.

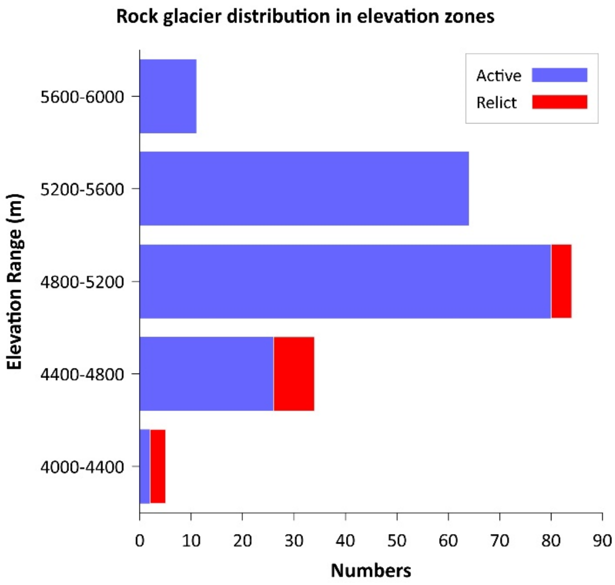

Figure 5. Distribution of active and relict rock glaciers in different elevation zones.

A scatter plot (Figure 6a) between the elevation and aspect of the rock glaciers indicates that active rock glaciers are located at a higher elevation compared to the relict rock glaciers, with few exceptions. Moreover, active rock glaciers are mostly present in the northern slopes (N, NE, and NW). Furthermore, another scatter plot of the MAAT against the PISR, shown in Figure 6b, shows that most of the rock glacier sites experience higher insolation in the range of 600–700 kWh m^{-2}, but their corresponding mean annual average temperatures vary in the range of 0 to −10 °C at the elevation where the rock glaciers are located. This gives some insight into how temperature strongly influences the presence or absence of permafrost near the rock glaciers.

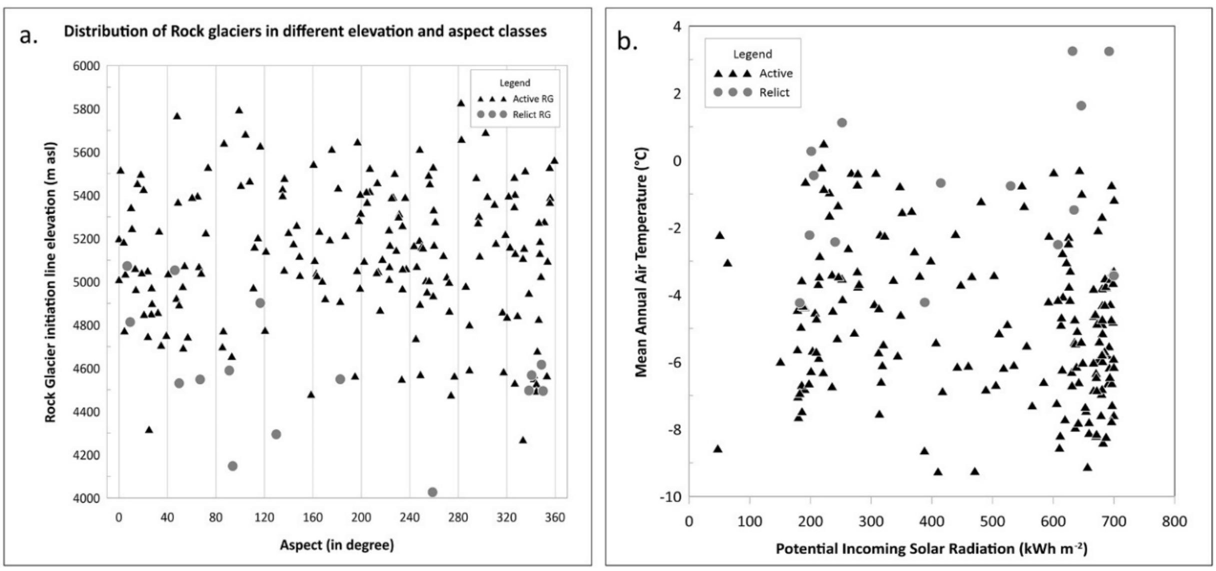

Figure 6. (**a**) Difference in relict and active rock glacier initiation line elevation and orientation; (**b**) Mean annual air temperature and incoming solar radiation.

The distribution of active and relict rock glaciers in the study area is shown in Figure 7.

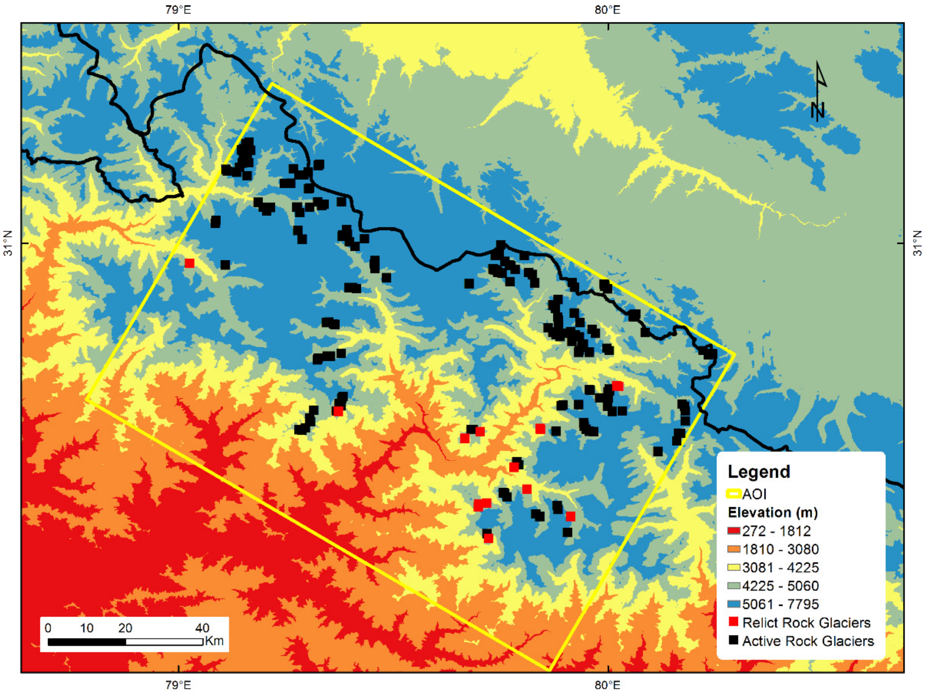

Figure 7. Distribution of rock glaciers in the study area.

4.2. Logistic Regression Models

Three logistic regression models (LRM-MAAT, LRM-LST, and LRM-SC) were developed from a dataset of 183 active and 15 relict rock glaciers (dependent variable) and their corresponding topoclimatic parameters (independent variables) to predict the spatial distribution of permafrost in the study area. The overall classification accuracy was 92.4%, 82.4%, and 91.9% for the LRM-MAAT, LRM-LST, and LRM-SC models, respectively, which signifies that the models' predictions are very reliable. All the models were statistically significant compared to the null models (p-value < 0.001). Nearly 1000 bootstrap samples were used to generate the model outputs.

In the MAAT-based logistic regression model (LRM-MAAT), it is very evident from their B_z (coefficient) values that both MAAT ($B_z = -0.777$) and PISR ($B_z = -0.001$) are negatively related to the presence of permafrost in the area. The coefficient of MAAT is highly significant ($p < 0.001$), which shows its control over the prediction of the distribution of permafrost over other predictor variables. The statistical outcomes of the model are given in Table 3.

Table 3. Statistical outcomes from LRM-MAAT, including the coefficient (B_z), bias (°C), and standard error (SE).

					95% Confidence Interval of B_z	
	B_z	Bias (°C)	SE (°C)	p-value	Lower	Upper
MAAT	−0.777	−0.072	0.212	0.001	−1.325	−0.540
PISR	−0.001	0.000	0.003	0.006	−0.004	0.005
Aspect	0.004	0.001	0.008	0.089	−0.001	0.013
Constant	7.689	0.022	1.295	0.004	4.321	11.754

In the LST-based model, the output results are similar to the MAAT-based model, where LST is negatively related ($B_z = -0.706$) to the presence of permafrost, along with

PISR (B_z = −0.002), which means the lower the values of land surface temperature, the higher the probability of the occurrence of permafrost, and there is a strong effect (p = 0.001). The statistical outcomes of the model are given in Table 4.

Table 4. Statistical outcomes from LRM-LST, including the coefficient (B_z), bias (°C), and standard error (SE).

					95% Confidence Interval of B_z	
	B_z	Bias (°C)	SE (°C)	p-value	Lower	Upper
LST	−0.706	−0.048	0.143	0.001	−0.987	−0.350
PISR	−0.002	0.000	0.002	0.004	−0.003	0.005
Aspect	0.001	0.000	0.005	0.064	−0.005	0.010
Constant	3.231	0.063	0.998	0.001	1.343	6.154

In the snow-cover-based logistic regression model (LRM-SC), the model coefficients are different than the other two models. In this model, the snow cover is positively related (Bz = 0.789) to the presence of permafrost, as a higher value of the NDSI of the snow-covered layer signifies a higher snow content and perennially snow-covered areas, which has significant control (p = 0.001) over the permafrost areas. Table 5 shows the statistical outcomes of the model.

Table 5. Statistical outcomes from LRM-SC, including the coefficient (B_z), bias, and standard error (SE).

					95% Confidence Interval of B_z	
	B_z	Bias	SE	p-value	Lower	Upper
Snow Cover	0.789	0.009	0.054	0.001	0.312	0.956
PISR	−0.001	0.000	0.002	0.005	−0.003	0.005
Aspect	0.003	0.001	0.005	0.038	0.053	0.266
Constant	3.514	0.106	1.872	0.028	0.438	6.327

4.3. Permafrost Distribution Map Interpretation

The permafrost distribution map developed from LRM-MAAT indicated that the minimum elevation at which the permafrost is present is ~4800 m, below which there is no presence of permafrost in the study area. High-altitude areas with elevations of 5900 m and above and with corresponding MAAT values ranging from −8 to −18 °C show a high probability of permafrost occurrence. As the elevation decreases, the MAAT also rises gradually, resulting in a lower probability of permafrost presence down the slopes of the mountains and in the valley region. From the modeled map, it was observed that certain rock glacier locations violated the assumption of active rock glaciers being an indicator of permafrost presence, as 11 active rock glaciers are outside the fringes of the permafrost distribution in the study area, as predicted by this model.

Another permafrost distribution map was developed using the coefficients from LRM-LST. In this predicted map, a noticeable change was found in the aerial expanse of the permafrost presence in the study area. The presence of permafrost in the area corresponds with an LST of −5 °C and below. The area coverage is decreased compared to the map developed from LRM-MAAT.

The predicted map from the snow-cover-based logistic regression model (LRM-SC), exhibits a larger coverage area with a high probability of permafrost presence in the study area compared to the other two models. The lower elevation limit of the permafrost areas is 3700 m. The predicted permafrost distribution map also covers all the mapped active rock glaciers in the study area, conforming with the assumption of our study. This proves that snow cover has a significant role in modeling the presence of permafrost in the alpine environment.

The permafrost zonation maps from different logistic regression models are shown in Figure 8.

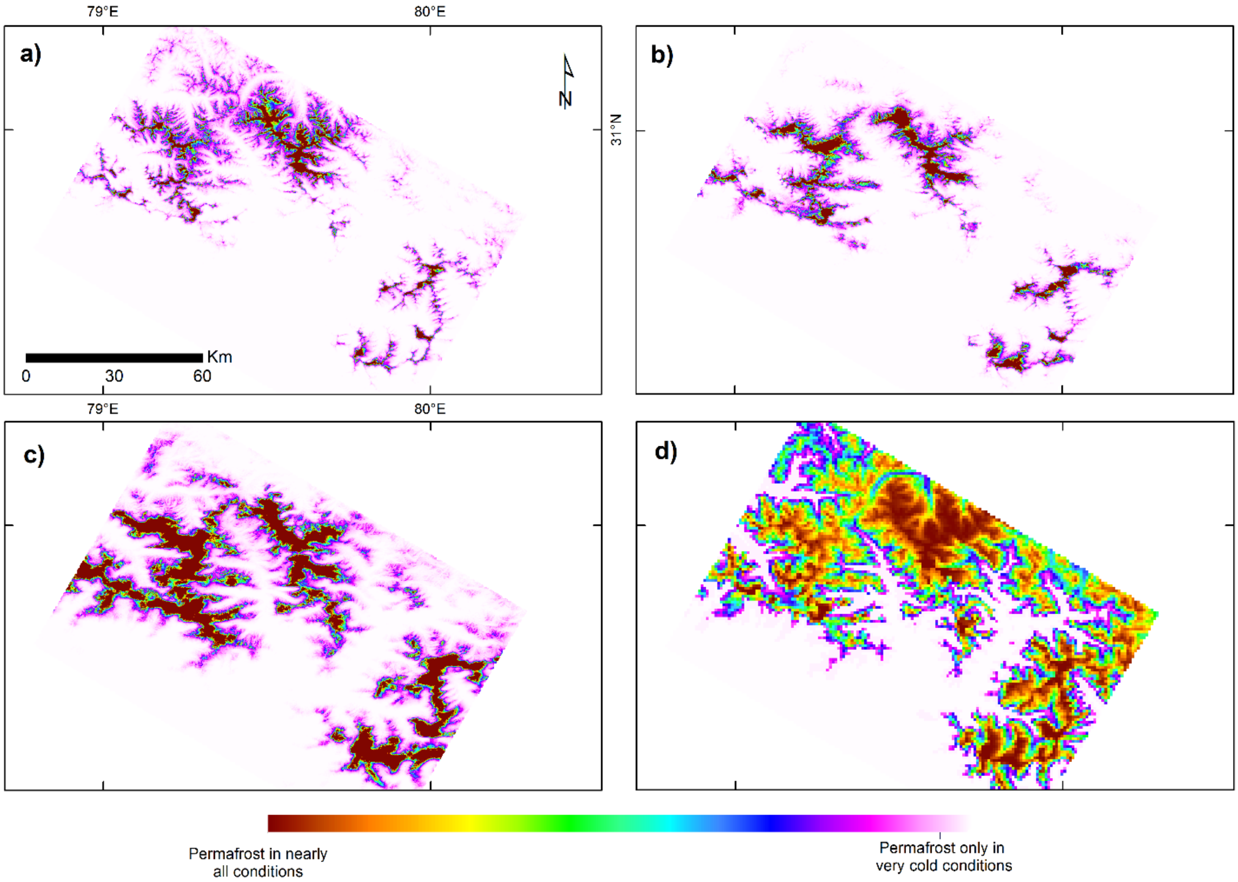

Figure 8. Permafrost zonation maps derived from logistic regression models: (**a**) LRM-MAAT; (**b**) LRM-LST; (**c**) LRM-SC; (**d**) PZI map.

The area under the curve (AUC) scores of the different models signify their performance and reliability in predicting the output. LRM-MAAT has the highest area under the curve (0.902), followed by LRM-LST (0.866) and LRM-SC (0.777). Though the snow-cover-based model has a low AUC score, the prediction of the permafrost distribution by the model satisfies our assumption, as shown in Table 6 and Figure 9.

Table 6. Area under the ROC curves from different models.

				Asymptotic 95% Confidence Interval	
Model	**Area**	**Std. Error**	**Asymptotic Sig.**	**Lower Bound**	**Upper Bound**
LRM-MAAT	0.902	0.030	0.000	0.843	0.962
LRM-LST	0.866	0.034	0.000	0.798	0.933
LRM-SC	0.777	0.061	0.000	0.657	0.897

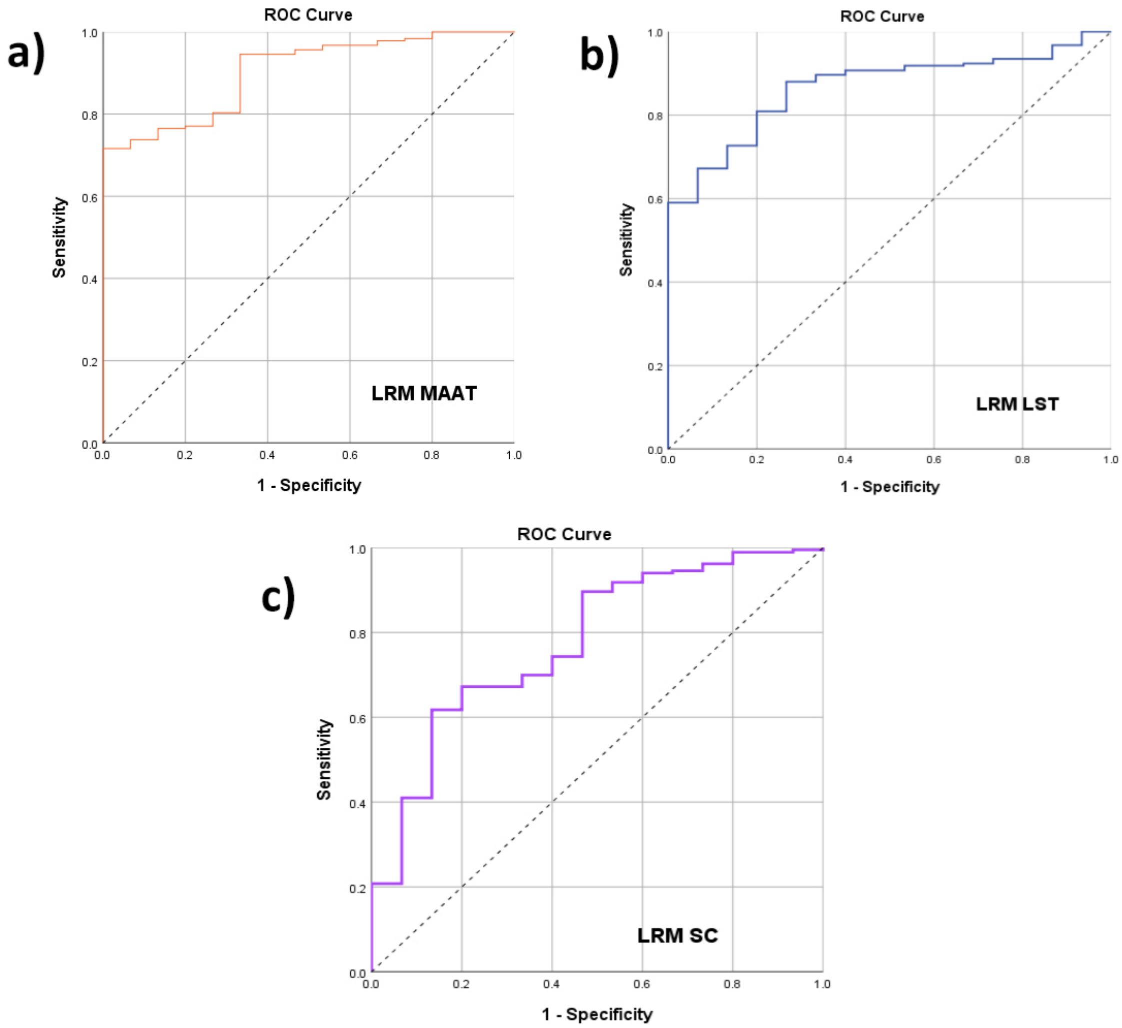

Figure 9. ROC curves for (**a**) LRM MAAT; (**b**) LRM LST; and (**c**) LRM SC.

5. Discussion

The permafrost zonation index (PZI) is a global map of permafrost extent that was developed by Gruber [34] based on an empirical relationship between the air temperature and permafrost occurrence. It has a spatial resolution of <1 km globally. The PZI helps to understand the spatial extent of permafrost on a coarser level, although it has its own limitations when considered at a local level since it only focuses on a single parameter, i.e., temperature. The present study compared and validated the output of the LRM-MAAT model with the PZI, and our modeled map was in sync with the PZI map [34]. When compared to PZI maps, the modeled findings appear to underestimate the spatial arrangement of permafrost, which is mainly due to the coarse spatial resolution of the dataset used to develop the regression model, as shown in Figure 10.

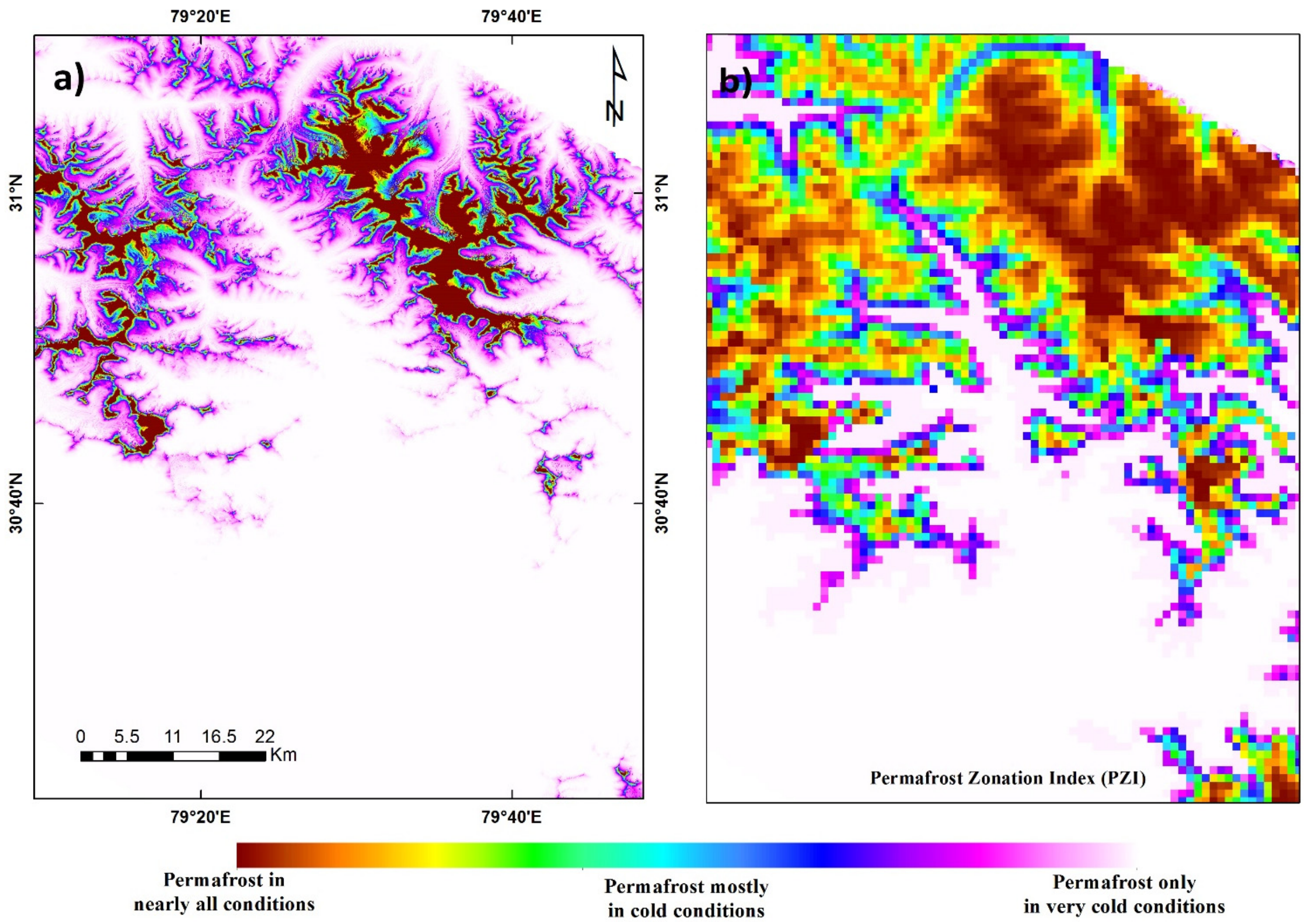

Figure 10. Comparison of (**a**) LRM-MAAT and (**b**) the PZI map over a small area.

Previous studies on permafrost distribution mapping in the Himalayan region used various techniques, namely statistical modeling and AHP [30–33]. Haq et al. [32] mapped the permafrost distribution in the Sikkim Himalayas based on logistic regression modeling using the MAAT and PISR. The distribution of rock glaciers was shown to be strongly influenced by elevation and aspect. The presence of permafrost is favored by topoclimatic conditions over 5000 m a.s.l. The study also found that the Sentinel-2 datasets are useful for studying rock glaciers in the Himalayas. Khan et al. [33] presented a permafrost distribution map for Jammu and Kashmir Union Territory (UT) and Ladakh UT, where they used AHP modeling using parameters such as the biannual mean air temperature (BMAT), PISR, aspect, slope, and land use/land cover. Permafrost is primarily governed by temperature, with some indirect influences coming from other ground factors (e.g., land use/land cover, surface properties, and PISR). The higher reaches with an extremely cold and dry climate were identified to be favorable areas for the occurrence of permafrost. Baral et al. [30] developed permafrost zonation maps for the Uttarakhand state, considering different rock glacier types based on their origins and statistical relationships with the MAAT, PISR, and LST. The majority of rock glaciers are found at elevations of more than 4000 m a.s.l. This study also suggested that logistic regression models can create reliable estimations of permafrost probability.

In the present study, all three models (i.e., LRM-MAAT, LRM-LST, and LRM-SC) showed the influence of different topoclimatic variables in predicting the permafrost distribution. None of the studies mentioned above considered the influence of snow cover insulating the permafrost below the ground. The present study developed a first-order permafrost distribution modeled map using the mean snow cover over 21 years, which rendered some promising results and supports the assumption of the presence of permafrost near the initiation points of active rock glaciers. The thermal insulation effect of snow cover directly influences the ground surface temperature. Various studies have suggested that snow cover variations affect the ground thermal regime in permafrost areas [60,61]. Snow cover in the summer may lead to decreased ground surface temperature compared to the increased air temperature and may help in shortening the thawing season, which in turn reduces active layer thawing propagation. Zhang [60] described in detail how snow cover plays a significant role in controlling the permafrost temperature from continuous permafrost areas to seasonally frozen ground. Therefore, this study considers snow cover a significant parameter when modeling permafrost distribution. Even though the classification accuracy of LRM-SC is comparable to the LRM-MAAT model, its AUC score is relatively low compared to LRM-MAAT. The classification accuracy of a classifier is computed at a threshold value of 0.5, whereas the AUC is computed as the accuracies averaged across all possible threshold values. LRM-SC yields a lower AUC score, predominantly because of the imbalance in class representation (active and relict rock glaciers). The LRM-SC model is capable of distinguishing between classes (0 as 0 and 1 as 1) with 77.7% prediction accuracy, which is well above random guessing (AUC = 0.5). In this study, we mainly focused on classification accuracy, which signifies a model's ability to classify in a binary classification scenario. Field measurements of snow depth and the duration of snow cover are also needed to understand their effects on permafrost depth in mountain permafrost regions, especially in the Himalayas. Several studies have also shown that remote sensing techniques can be utilized to monitor permafrost [62,63]. However, the efficacy of optical remote sensing for permafrost monitoring is restricted since permafrost occurs mostly below the surface. As a result, passive microwave remote sensing brightness temperature data products and ground surface soil freeze/thaw states derived by the dual-index algorithm (DIA) would be effective for mapping the distribution of permafrost [62]. Notably, studies on monitoring the thermal status of permafrost are severely underrepresented due to the limited accessibility of significant areas of permafrost landscapes [64]. Therefore, future studies should focus on the use of emerging tools (e.g., the Google Earth Engine), approaches (e.g., deep learning algorithms), and satellite data (e.g., Sentinel, Synthetic Aperture Radar, etc.) to investigate the extent of permafrost and its environmental repercussions (e.g., thermokarst features and greenhouse gas emissions).

6. Conclusions

In the present study, three logistic regression models were developed and compared based on the statistical relationship between active and relict rock glaciers and their corresponding topoclimatic variables to estimate the presence of permafrost in the Alaknanda Valley, Uttarakhand, India. The study produced a first-order permafrost distribution map of the Alaknanda Valley, Uttarakhand, India, based on 21 years of mean snow cover MODIS data.

The results from the models show that permafrost in the study area exists at a mean altitude of ~4250 m and above. The comparison among the different permafrost distribution maps indicated that snow cover can be one of the significant climatic parameters that predicts permafrost in the Himalayan environment, in addition to the mean annual air temperature and the land surface temperature. The developed models were validated with a global PZI map, which was in good agreement with the results of the study.

The statistical modeling of remote sensing data incorporating rock glaciers can significantly contribute towards the study of permafrost in the Himalayan region. The accuracy of the models would depend on the correctness of manually identified rock glaciers and their types. Therefore, further field validation and sampling of rock glaciers are encouraged to improve model accuracy, along with field validation of the predicted permafrost distribution map.

Author Contributions: A.C.P., T.G. and B.R.P.: Conceptualization, Investigation, Methodology, Software, Analysis, Visualization, Writing—original draft, and Writing—review and editing. C.S.D. and R.K.T.: Methodology, Software, Supervision, Analysis, Visualization, Writing—original draft, and Writing—review and editing. All authors have read and agreed to the published version of the manuscript.

Funding: This research received funding from the ISRO's Disaster Management Support Programme (DMSP) project (grant IIRS/DO/DMSP-ASCB/AS/2022/07).

Institutional Review Board Statement: Not applicable.

Informed Consent Statement: Not applicable.

Data Availability Statement: Publicly available datasets were analyzed in this study, and they can be accessed from the sources given in Table 1.

Acknowledgments: The authors thank NASA, USGS, and WordClim for providing the data free of cost.

Conflicts of Interest: The authors declare no conflict of interest.

References

1. French, H.M. *The Periglacial Environment*, 4th ed.; John Wiley & Sons: Hoboken, NJ, USA, 2017; ISBN 978-1-119-13278-3.
2. Kitover, D.C.; van Balen, R.T.; Vandenberghe, J.; Roche, D.M.; Renssen, H. LGM Permafrost Thickness and Extent in the Northern Hemisphere Derived from the Earth System Model *i* LOVECLIM: LGM Permafrost Thickness and Extent Using *i* LOVECLIM. *Permafr. Periglac. Process.* **2016**, *27*, 31–42. [CrossRef]
3. Li, Y.; Conway, D.; Xiong, W.; Gao, Q.; Wu, Y.; Wan, Y.; Li, Y.; Zhang, S. Effects of Climate Variability and Change on Chinese Agriculture: A Review. *Clim. Res.* **2011**, *50*, 83–102. [CrossRef]
4. Boike, J.; Juszak, I.; Lange, S.; Chadburn, S.; Burke, E.; Overduin, P.P.; Roth, K.; Ippisch, O.; Bornemann, N.; Stern, L.; et al. A 20-Year Record (1998–2017) of Permafrost, Active Layer and Meteorological Conditions at a High Arctic Permafrost Research Site (Bayelva, Spitsbergen). *Earth Syst. Sci. Data* **2018**, *10*, 355–390. [CrossRef]
5. Cao, B.; Zhang, T.; Wu, Q.; Sheng, Y.; Zhao, L.; Zou, D. Permafrost Zonation Index Map and Statistics over the Qinghai-Tibet Plateau Based on Field Evidence. *Permafr. Periglac. Process.* **2019**, *30*, 178–194. [CrossRef]
6. IPCC. *The Ocean and Cryosphere in a Changing Climate: Special Report of the Intergovernmental Panel on Climate Change*, 1st ed.; Cambridge University Press: Cambridge, UK, 2022; ISBN 978-1-00-915796-4.
7. Haeberli, W.; Guodong, C.; Gorbunov, A.P.; Harris, S.A. Mountain Permafrost and Climatic Change. *Permafr. Periglac. Process.* **1993**, *4*, 165–174. [CrossRef]
8. Harris, C.; Arenson, L.U.; Christiansen, H.H.; Etzelmüller, B.; Frauenfelder, R.; Gruber, S.; Haeberli, W.; Hauck, C.; Hölzle, M.; Humlum, O.; et al. Permafrost and Climate in Europe: Monitoring and Modelling Thermal, Geomorphological and Geotechnical Responses. *Earth-Sci. Rev.* **2009**, *92*, 117–171. [CrossRef]
9. Yang, M.; Nelson, F.E.; Shiklomanov, N.I.; Guo, D.; Wan, G. Permafrost Degradation and Its Environmental Effects on the Tibetan Plateau: A Review of Recent Research. *Earth-Sci. Rev.* **2010**, *103*, 31–44. [CrossRef]
10. Shugar, D.H.; Jacquemart, M.; Shean, D.; Bhushan, S.; Upadhyay, K.; Sattar, A.; Schwanghart, W.; McBride, S.; de Vries, M.V.W.; Mergili, M.; et al. A Massive Rock and Ice Avalanche Caused the 2021 Disaster at Chamoli, Indian Himalaya. *Science* **2021**, *373*, 300–306. [CrossRef]
11. Das, S.; Sarkar, S.; Kanungo, D.P. A Critical Review on Landslide Susceptibility Zonation: Recent Trends, Techniques, and Practices in Indian Himalaya. *Nat. Hazards* **2022**. [CrossRef]
12. Parida, B.; Behera, S.; Bakimchandra, O.; Pandey, A.; Singh, N. Evaluation of Satellite-Derived Rainfall Estimates for an Extreme Rainfall Event over Uttarakhand, Western Himalayas. *Hydrology* **2017**, *4*, 22. [CrossRef]
13. Singh, N.; Shekhar, M.; Parida, B.R.; Gupta, A.K.; Sain, K.; Rai, S.K.; Bräuning, A.; Singh Charkaborty, J.; Sharma, V.; Kamal Tiwari, R.; et al. Tree-Ring Isotopic Records Suggest Seasonal Importance of Moisture Dynamics Over Glacial Valleys of the Central Himalaya. *Front. Earth Sci.* **2022**, *10*, 868357. [CrossRef]
14. Barsch, D. *Rockglaciers: Indicators for the Present and Former Geoecology in High Mountain Environments*; Springer Series in Physical Environment; Springer: Berlin, Germany; New York, NY, USA, 1996; ISBN 978-3-540-60742-7.
15. Haeberli, W.; Hallet, B.; Arenson, L.; Elconin, R.; Humlum, O.; Kääb, A.; Kaufmann, V.; Ladanyi, B.; Matsuoka, N.; Springman, S.; et al. Permafrost Creep and Rock Glacier Dynamics. *Permafr. Periglac. Process.* **2006**, *17*, 189–214. [CrossRef]
16. Barsch, D. Permafrost Creep and Rockglaciers. *Permafr. Periglac. Process.* **1992**, *3*, 175–188. [CrossRef]
17. Frehner, M.; Ling, A.H.M.; Gärtner-Roer, I. Furrow-and-Ridge Morphology on Rockglaciers Explained by Gravity-Driven Buckle Folding: A Case Study From the Murtèl Rockglacier (Switzerland): Rockglacier Furrow-and-Ridge Morphology Explained by Buckle Folding. *Permafr. Periglac. Process.* **2015**, *26*, 57–66. [CrossRef]

18. Azam, M.F.; Ramanathan, A.; Wagnon, P.; Vincent, C.; Linda, A.; Berthier, E.; Sharma, P.; Mandal, A.; Angchuk, T.; Singh, V.B.; et al. Meteorological Conditions, Seasonal and Annual Mass Balances of Chhota Shigri Glacier, Western Himalaya, India. *Ann. Glaciol.* **2016**, *57*, 328–338. [CrossRef]
19. Sood, V.; Tiwari, R.K.; Singh, S.; Kaur, R.; Parida, B.R. Glacier Boundary Mapping Using Deep Learning Classification over Bara Shigri Glacier in Western Himalayas. *Sustainability* **2022**, *14*, 13485. [CrossRef]
20. Jain, S.K.; Mir, R.A. Glacier and Glacial Lake Classification for Change Detection Studies Using Satellite Data: A Case Study from Baspa Basin, Western Himalaya. *Geocarto Int.* **2019**, *34*, 391–414. [CrossRef]
21. Akhtar, M.; Ahmad, N.; Booij, M.J. The Impact of Climate Change on the Water Resources of Hindukush–Karakorum–Himalaya Region under Different Glacier Coverage Scenarios. *J. Hydrol.* **2008**, *355*, 148–163. [CrossRef]
22. Bhambri, R.; Bolch, T.; Chaujar, R.K.; Kulshreshtha, S.C. Glacier Changes in the Garhwal Himalaya, India, from 1968 to 2006 Based on Remote Sensing. *J. Glaciol.* **2011**, *57*, 543–556. [CrossRef]
23. Azócar, G.F.; Brenning, A.; Bodin, X. Permafrost Distribution Modelling in the Semi-Arid Chilean Andes. *Cryosphere* **2017**, *11*, 877–890. [CrossRef]
24. Marcer, M.; Bodin, X.; Brenning, A.; Schoeneich, P.; Charvet, R.; Gottardi, F. Permafrost Favorability Index: Spatial Modeling in the French Alps Using a Rock Glacier Inventory. *Front. Earth Sci.* **2017**, *5*, 105. [CrossRef]
25. Sattler, K.; Anderson, B.; Mackintosh, A.; Norton, K.; de Róiste, M. Estimating Permafrost Distribution in the Maritime Southern Alps, New Zealand, Based on Climatic Conditions at Rock Glacier Sites. *Front. Earth Sci.* **2016**, *4*, 4. [CrossRef]
26. Zhang, Z.; Wang, M.; Wu, Z.; Liu, X. Permafrost Deformation Monitoring Along the Qinghai-Tibet Plateau Engineering Corridor Using InSAR Observations with Multi-Sensor SAR Datasets from 1997–2018. *Sensors* **2019**, *19*, 5306. [CrossRef] [PubMed]
27. Gruber, S.; Fleiner, R.; Guegan, E.; Panday, P.; Schmid, M.-O.; Stumm, D.; Wester, P.; Zhang, Y.; Zhao, L. Review Article: Inferring Permafrost and Permafrost Thaw in the Mountains of the Hindu Kush Himalaya Region. *Cryosphere* **2017**, *11*, 81–99. [CrossRef]
28. Hassan, J.; Chen, X.; Muhammad, S.; Bazai, N.A. Rock Glacier Inventory, Permafrost Probability Distribution Modeling and Associated Hazards in the Hunza River Basin, Western Karakoram, Pakistan. *Sci. Total Environ.* **2021**, *782*, 146833. [CrossRef] [PubMed]
29. Schmid, M.-O.; Baral, P.; Gruber, S.; Shahi, S.; Shrestha, T.; Stumm, D.; Wester, P. Assessment of Permafrost Distribution Maps in the Hindu Kush Himalayan Region Using Rock Glaciers Mapped in Google Earth. *Cryosphere* **2015**, *9*, 2089–2099. [CrossRef]
30. Baral, P.; Haq, M.A.; Yaragal, S. Assessment of Rock Glaciers and Permafrost Distribution in Uttarakhand, India. *Permafr. Periglac. Process.* **2020**, *31*, 31–56. [CrossRef]
31. Allen, S.K.; Fiddes, J.; Linsbauer, A.; Randhawa, S.S.; Saklani, B.; Salzmann, N. Permafrost Studies in Kullu District, Himachal Pradesh. *Curr. Sci.* **2016**, *111*, 550. [CrossRef]
32. Haq, M.A.; Baral, P. Study of Permafrost Distribution in Sikkim Himalayas Using Sentinel-2 Satellite Images and Logistic Regression Modelling. *Geomorphology* **2019**, *333*, 123–136. [CrossRef]
33. Khan, M.A.R.; Singh, S.; Pandey, P.; Bhardwaj, A.; Ali, S.N.; Chaturvedi, V.; Ray, P.K.C. Modelling Permafrost Distribution in Western Himalaya Using Remote Sensing and Field Observations. *Remote Sens.* **2021**, *13*, 4403. [CrossRef]
34. Gruber, S. Derivation and Analysis of a High-Resolution Estimate of Global Permafrost Zonation. *Cryosphere* **2012**, *6*, 221–233. [CrossRef]
35. Obu, J.; Westermann, S.; Bartsch, A.; Berdnikov, N.; Christiansen, H.H.; Dashtseren, A.; Delaloye, R.; Elberling, B.; Etzelmüller, B.; Kholodov, A.; et al. Northern Hemisphere Permafrost Map Based on TTOP Modelling for 2000–2016 at 1 Km2 Scale. *Earth-Sci. Rev.* **2019**, *193*, 299–316. [CrossRef]
36. Ali, S.N.; Quamar, M.; Phartiyal, B.; Sharma, A. Need for Permafrost Researches in Indian Himalaya. *J. Clim. Chang.* **2018**, *4*, 33–36. [CrossRef]
37. Fick, S.E.; Hijmans, R.J. WorldClim 2: New 1-km Spatial Resolution Climate Surfaces for Global Land Areas. *Int. J. Climatol.* **2017**, *37*, 4302–4315. [CrossRef]
38. Zhengming, W.; Simon, H.; Glynn, H. MODIS/Terra Land Surface Temperature/Emissivity 8-Day L3 Global 1km SIN Grid V061. 2021. Available online: https://lpdaac.usgs.gov/products/mod11a2v006/ (accessed on 4 June 2022).
39. Hall, D.K.; Riggs, G.A.; Solomonson, V. NASA MODAPS SIPS MODIS/Terra Snow Cover Daily L3 Global 500 m SIN Grid. 2015. Available online: https://nsidc.org/data/mod10a1/versions/6 (accessed on 2 June 2022).
40. NASA/METI/AIST/Japan Spacesystems and U.S./Japan ASTER Science Team ASTER Global Digital Elevation Model V003. 2019. Available online: https://lpdaac.usgs.gov/products/astgtmv003/ (accessed on 7 June 2022).
41. Earth Resources Observation and Science (EROS) Center Global 30 Arc-Second Elevation (GTOPO30). 2017. Available online: https://earthexplorer.usgs.gov/ (accessed on 4 June 2022).
42. Hachem, S.; Allard, M.; Duguay, C. Using the MODIS Land Surface Temperature Product for Mapping Permafrost: An Application to Northern Québec and Labrador, Canada: Using the MODIS Land Surface Temperature Product for Mapping Permafrost. *Permafr. Periglac. Process.* **2009**, *20*, 407–416. [CrossRef]
43. Westermann, S.; Langer, M.; Boike, J. Spatial and Temporal Variations of Summer Surface Temperatures of High-Arctic Tundra on Svalbard—Implications for MODIS LST Based Permafrost Monitoring. *Remote Sens. Environ.* **2011**, *115*, 908–922. [CrossRef]
44. Yin, G.; Zheng, H.; Niu, F.; Luo, J.; Lin, Z.; Liu, M. Numerical Mapping and Modeling Permafrost Thermal Dynamics across the Qinghai-Tibet Engineering Corridor, China Integrated with Remote Sensing. *Remote Sens.* **2018**, *10*, 2069. [CrossRef]

45. Guglielmin, M.; Aldighieri, B.; Testa, B. PERMACLIM: A Model for the Distribution of Mountain Permafrost, Based on Climatic Observations. *Geomorphology* **2003**, *51*, 245–257. [CrossRef]
46. Hall, D.K.; Riggs, G.A. Normalized-Difference Snow Index (NDSI). In *Encyclopedia of Snow, Ice and Glaciers*; Singh, V.P., Singh, P., Haritashya, U.K., Eds.; Encyclopedia of Earth Sciences Series; Springer: Dordrecht, The Netherlands, 2011; pp. 779–780. ISBN 978-90-481-2641-5.
47. Martin, H. *Permafrost und Gletscher im Oberengadin: Grundlagen und Anwendungsbeispiele für automatisierte Schätzverfahren*; ETH: Zurich, Switzerland, 1994; p. 130S.
48. Bharti, R.R.; Adhikari, B.S.; Rawat, G.S. Assessing Vegetation Changes in Timberline Ecotone of Nanda Devi National Park, Uttarakhand. *Int. J. Appl. Earth Obs. Geoinf.* **2012**, *18*, 472–479. [CrossRef]
49. Maheshwari, A. Snow Leopard (Panthera Uncia) Surveys in the Western Himalayas, India. *J. Ecol. Nat. Environ.* **2013**, *5*, 303–309. [CrossRef]
50. López-Moreno, J.I.; Revuelto, J.; Gilaberte, M.; Morán-Tejeda, E.; Pons, M.; Jover, E.; Esteban, P.; García, C.; Pomeroy, J.W. The Effect of Slope Aspect on the Response of Snowpack to Climate Warming in the Pyrenees. *Theor. Appl. Climatol.* **2014**, *117*, 207–219. [CrossRef]
51. Kääb, A.; Weber, M. Development of Transverse Ridges on Rock Glaciers: Field Measurements and Laboratory Experiments: Transverse Ridges on Rock Glaciers. *Permafr. Periglac. Process.* **2004**, *15*, 379–391. [CrossRef]
52. Baroni, C.; Carton, A.; Seppi, R. Distribution and Behaviour of Rock Glaciers in the Adamello–Presanella Massif (Italian Alps). *Permafr. Periglac. Process.* **2004**, *15*, 243–259. [CrossRef]
53. Potter, N., Jr.; Steig, E.J.; Clark, D.H.; Speece, M.A.; Clark, G.M.; Updike, A.B. Galena Creek Rock Glacier Revisited—New Observations on an Old Controversy. *Geogr. Ann. Ser. Phys. Geogr.* **1998**, *80*, 251–265. [CrossRef]
54. Janke, J.R.; Regmi, N.R.; Giardino, J.R.; Vitek, J.D. 8.17 Rock Glaciers. In *Treatise on Geomorphology*; Elsevier: Amsterdam, The Netherlands, 2013; pp. 238–273. ISBN 978-0-08-088522-3.
55. Wahrhaftig, C.; Cox, A. Rock Glaciers in the Alaska Range. *Geol. Soc. Am. Bull.* **1959**, *70*, 383. [CrossRef]
56. Bodin, X.; Schoeneich, P.; Deline, P.; Ravanel, L.; Magnin, F.; Krysiecki, J.-M.; Echelard, T. Mountain Permafrost and Associated Geomorphological Processes: Recent Changes in the French Alps. *Rev. Géographie Alp.* **2015**, *103*, 1–17. [CrossRef]
57. Boeckli, L.; Brenning, A.; Gruber, S.; Noetzli, J. A Statistical Approach to Modelling Permafrost Distribution in the European Alps or Similar Mountain Ranges. *Cryosphere* **2012**, *6*, 125–140. [CrossRef]
58. Peng, C.-Y.J.; So, T.-S.H. Logistic Regression Analysis and Reporting: A Primer. *Underst. Stat.* **2002**, *1*, 31–70. [CrossRef]
59. Hosmer, D.W.; Lemeshow, S.; Sturdivant, R.X. *Applied Logistic Regression*, 3rd ed.; Wiley series in probability and statistics; Wiley: Hoboken, NJ, USA, 2013; ISBN 978-1-118-54838-7.
60. Zhang, T. Influence of the Seasonal Snow Cover on the Ground Thermal Regime: An Overview: Snow Cover and Ground Thermal Regime. *Rev. Geophys.* **2005**, *43*, RG4002. [CrossRef]
61. Hrbáček, F.; Engel, Z.; Kňažková, M.; Smolíková, J. *Effect of Ephemeral Snow Cover on the Active Layer Thermal Regime Andthickness on CALM-S JGM Site, James Ross Island, Eastern Antarctic Peninsula*; Frozen Ground/Antarctic: Gottingten, Germany, 2021.
62. Gao, H.; Nie, N.; Zhang, W.; Chen, H. Monitoring the Spatial Distribution and Changes in Permafrost with Passive Microwave Remote Sensing. *ISPRS J. Photogramm. Remote Sens.* **2020**, *170*, 142–155. [CrossRef]
63. Wang, J.; Jiang, L.; Wu, S.; Zhang, C.; Chen, Y.; Li, H.; Yang, J.; Pan, F.; Cui, H. Land Surface Freeze/Thaw Detection Over the Qinghai–Tibet Plateau Using FY-3/MWRI Data. *IEEE Trans. Geosci. Remote Sens.* **2022**, *60*, 4305017. [CrossRef]
64. Philipp, M.; Dietz, A.; Buchelt, S.; Kuenzer, C. Trends in Satellite Earth Observation for Permafrost Related Analyses—A Review. *Remote Sens.* **2021**, *13*, 1217. [CrossRef]